Contents lists available at SciVerse ScienceDirect

Chemical Engineering Research and Design

journal homepage: www.elsevier.com/locate/cherd

Modeling of Rayleigh convection in gas–liquid interfacial mass transfer using lattice Boltzmann method

Bo Fu, Botan Liu, Xigang Yuan, Shuyong Chen, Kuotsung Yu*

State Key Laboratory of Chemical Engineering, School of Chemical Engineering and Technology, Tianjin University, Tianjin 300072, China

ABSTRACT

Interfacial Rayleigh convection can be generated by concentration gradient near the interface in mass transfer processes. In the present study, a 2D time-dependent lattice Boltzmann method (LBM) with a double distribution model was established for simulating the liquid-phase Rayleigh convection in the mass transfer process of CO_2 absorption into various solvents. Two random parameters P and C_D denoting respectively the possibility and the magnitude of concentration perturbation at interface were introduced to model the interfacial disturbance, which is known as one of the necessary conditions of onset of Rayleigh convection. The values of the parameters were identified ($0.05 \le P < 0.3$ and $0 < C_D \le 10^{-9}\,kg\,m^{-3}$) by comparing simulated critical onset times of the Rayleigh convection with the experimental result from Blair and Quinn (1969) and theoretical predictions proposed by Kim et al. (2006) and Tan and Thorpe (1992, 1999). The maximum penetration depths, maximum transient Rayleigh numbers, and critical times for the onset of Rayleigh convection were obtained by the proposed model. The simulations captured the detailed information of the onset and the temporal–spatial evolution of Rayleigh convection, and gave the concentration contours of typical plume convection patterns which were well consistent with literatures. Enhancement of mass transfer by the Rayleigh convection was also demonstrated by comparing the simulated instantaneous mass flux across the interface with that predicted by penetration theory.

Keywords: Rayleigh convection; Lattice Boltzmann method; Mass transfer; Interfacial perturbation; Convection onset time

1. Introduction

Rayleigh convection is an interfacial turbulent phenomenon usually observed in mass transfer processes like distillation, absorption, etc. (Grahn, 2006; Poodt et al., 2008; Farajzadeh et al., 2009; Chen, 2010) and known as influential to the mass transfer (Sun and Yu, 2006). In an interfacial mass transfer process, the concentration gradient of the transferred component near the interface may generate Rayleigh instability if the concentration gradient leads to a density gradient that directs oppositely to the direction of the gravity, and at the same time disturbance exists at the interface (Rayleigh, 1916). The previous experimental and theoretical studies on Rayleigh convection covered the observation of the Rayleigh convection patterns (Okhotsimskiis and Hozawa, 1998; Kutepov et al., 2001; Arendt et al., 2004), measurement of the enhanced mass transfer rate (Sun et al., 2002; Chen, 2010) and prediction of onset of Rayleigh convection (Sun and Fahmy, 2006). Several instability analysis approaches (Tan and Thorpe, 1992, 1999; Kurenkova et al., 2003; Kim et al., 2006; Riaz et al., 2006; Barbosa et al., 2008; Hassanzadeh et al., 2009; Kim and Lee, 2009; Tan et al., 2009, 2010; Sun, 2012) have been proposed for Rayleigh convection in mass transfer systems.

Numerical simulation becomes the important method to investigate the interfacial Rayleigh convection in mass transfer processes, and most of previous works on the Rayleigh effect simulation in the literatures applied traditional computational fluid dynamics (CFD) methods (Sha et al., 2002; Farajzadeh et al., 2007; Hidalgo and Carrera, 2009). Recently, Lattice Boltzmann Method (LBM) has been shown to be an effective approach to simulate fluid flow and transport phenomena, especially in capturing characteristics of mesoscale phenomena like interfacial turbulence (Chang and Alexander, 2006). The LBM has been successfully applied to

* *Corresponding author*. Tel.: +86 22 27402786; fax: +86 22 27404496.
E-mail address: yuanxg@tju.edu.cn (X. Yuan).
Received 24 February 2012; Received in revised form 30 October 2012; Accepted 12 November 2012
0263-8762/$ – see front matter © 2012 The Institution of Chemical Engineers. Published by Elsevier B.V. All rights reserved.
http://dx.doi.org/10.1016/j.cherd.2012.11.006

Nomenclature

A_I	interfacial area (m^2)
Bi_D	transient Biot number for mass transfer
C	solute concentration in the solution ($kg\,m^{-3}$)
C_D	concentration perturbation magnitude ($kg\,m^{-3}$)
C_I	interfacial concentration ($kg\,m^{-3}$)
C_I'	concentration at the liquid surface ($kg\,m^{-3}$)
C^*	equilibrium concentration in liquid solution ($kg\,m^{-3}$)
C_0	initial concentration in the solution ($kg\,m^{-3}$)
c	lattice velocity set to unity
$\mathbf{c}_i$	discrete velocity vector for D2Q9 ($m\,s^{-1}$)
D_g	diffusion coefficient of solute in the gas ($m^2\,s^{-1}$)
D_l	diffusion coefficient of solute in the liquid ($m^2\,s^{-1}$)
$\boldsymbol{F}$	body force per unite volume of Rayleigh convection ($N\,m^{-3}$)
f	density distribution function of the solvent
f^{eq}	equilibrium density distribution function of the solvent
g	concentration distribution function of the solute
g^{eq}	equilibrium concentration distribution function of the solute
$\boldsymbol{g}$	acceleration due to gravity ($m\,s^{-2}$)
H	henry constant ($Pa\,m^3\,mol^{-1}$)
h	thickness of liquid layer (mm)
Ma	Marangoni number
N	mass flux across the interface ($kg\,m^{-2}\,s^{-1}$)
P	perturbation probability
R	gas constant ($J\,mol^{-1}\,K^{-1}$)
Ra	Rayleigh number
Ra_c	theoretical critical Rayleigh number
Ra_{max}	maximum transient Rayleigh number
Ra_z	transient Rayleigh number
T	temperature (K)
t	time (s)
t_c	critical onset time of Rayleigh convection (s)
$\boldsymbol{u}$	macroscopic velocity ($m\,s^{-1}$)
u_x	horizontal velocity ($m\,s^{-1}$)
$\boldsymbol{u}^*$	modified velocity in the equilibrium distribution function ($m\,s^{-1}$)
V	liquid volume (m^3)
$\boldsymbol{x}$	position vector
x	coordinate (mm)
y	coordinate (mm)
z	vertical distance from the interface (mm)
z_{max}	maximum penetration depth (mm)

Greek letters

δC	concentration perturbation ($kg\,m^{-3}$)
δt	time interval used in Eq. (13) to calculate the mass flux across interface (s)
ΔC	difference between the concentrations of pure solvent and saturated solution ($kg\,m^{-3}$)
Δt	lattice time step size (s)
Δx	lattice space step size, m
$\Delta\rho$	difference between the densities of pure solvent and saturated solution ($kg\,m^{-3}$)
μ_0	dynamic viscosity of the pure solvent (Pa s)
υ	kinematic viscosity ($m^2\,s^{-1}$)
ρ	macroscopic density ($kg\,m^{-3}$)
ρ_0	density of the pure solvent ($kg\,m^{-3}$)
τ	relaxation time
ω	weight factor

Subscripts

A	solvent
avg	average
B	solute
c	critical
g	gas
I	interface
i	discrete directions of D2Q9 model ($i = 1, 2, \ldots, 9$)
ins	instantaneous
l	liquid
max	maximum
t	time

Superscripts

eq	equilibrium
0	prediction by penetration theory

the simulation of natural convection caused by thermal effect (Shan, 1997; Mohamad et al., 2009; Mussa et al., 2011) and double-diffusive natural convection (Verhaeghe et al., 2007; Ma, 2009) caused by both temperature and concentration gradients. Fu et al. (2011) have simulated the Rayleigh convection generated by a local high concentration gradient in the gas–liquid mass transfer process of CO_2 absorption into liquid ethanol by using LBM. However, in real gas–liquid mass transfer processes, concentration gradient driven Rayleigh convection is generally known to be induced by interfacial disturbance in the presence of Rayleigh instability. The interfacial disturbance is definitely complex and random in nature.

The objective of this paper is to develop a perturbation model in the LBM frame and to identify the correspondent parameters. Liquid side Rayleigh convection in the gas–liquid mass transfer process of CO_2 absorption into quiescent solvents is simulated by the proposed model, which is a random perturbation model with two parameters mimicking the randomness of disturbances at the gas–liquid interface. The experimental result from Blair and Quinn (1969) and theoretical predictions proposed by Kim et al. (2006) and Tan and Thorpe (1992, 1999) on the critical conditions are employed in our analysis for identifying the right values of the parameters. A two-dimensional time-dependent LBM with a double distribution model is established and applied in our simulations. Based on the simulation, interfacial mass transfer behaviors are analyzed.

2. LBM for simulation of Rayleigh convection

2.1. Physical model

The two-dimensional computational domain in this study is shown in Fig. 1. The initially pure and quiescent liquid is confined in a rectangle domain. The upper boundary of the domain, a free surface of the liquid, is regarded as a gas–liquid

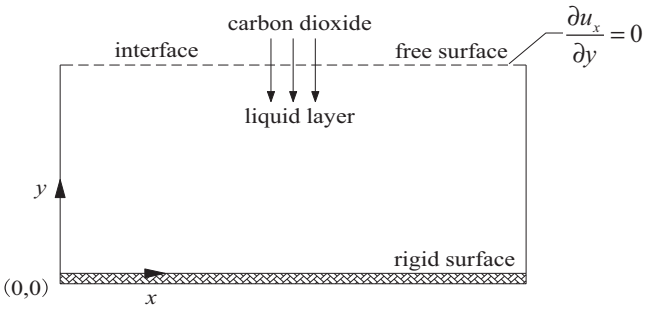

Fig. 1 – Computational domain of Rayleigh convection.

interface through which CO_2 is absorbed into the liquid. The lower boundary is assumed to be rigid surface.

The thermal effect of adsorption is neglected and the gas–liquid mass transfer process in simulations is assumed to be isothermal. Physical properties of the pure solvents and CO_2 saturated solutions at 298.15 K, 1.00 atm are listed in Table 1. For CO_2 absorption into all the solvents listed in Table 1, the interface is Rayleigh unstable ($Ra > 0$) and Marangoni stable ($Ma < 0$) (Okhotsimskiis and Hozawa, 1998).

2.2. *Double distribution model*

The LBM with a double distribution model (Inamuro et al., 2002) is implemented for simulating liquid-phase Rayleigh convection induced by interfacial mass transfer. The following assumptions are adopted in this paper:

(1) An isothermal binary miscible fluid mixture of solvent A and solute B is considered.
(2) The fraction of solute B is much smaller than that of solvent A.

In this paper, two-particle distribution functions f_{Ai} and g_{Bi}, representing respectively flow field and concentration field are solved simultaneously. Based on a standard D2Q9 lattice scheme (Qian et al., 1992) shown in Fig. 2, The LBGK evolution equations of the solvent and the solute without external forces can be expressed as (Bhatnagar et al., 1954):

$$f_{Ai}(x + c_i\Delta t, t + \Delta t) - f_{Ai}(x, t) = -\frac{1}{\tau_A}[f_{Ai}(x, t) - f_{Ai}^{eq}(x, t)] \quad (1)$$

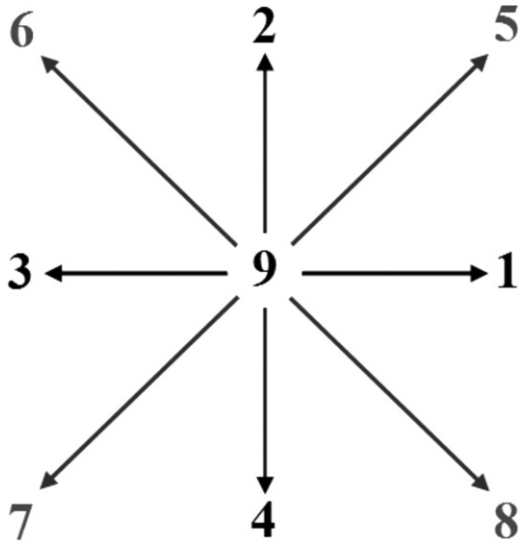

Fig. 2 – Two-dimensional nine-velocity (D2Q9) model.

$$g_{Bi}(x + c_i\Delta t, t + \Delta t) - g_{Bi}(x, t) = -\frac{1}{\tau_B}[g_{Bi}(x, t) - g_{Bi}^{eq}(x, t)] \quad (2)$$

The equilibrium distribution functions of A and B can be formulated as (Inamuro et al., 2002; Qian et al., 1992):

$$f_{Ai}^{eq} = \omega_i\rho_A\left[1 + \frac{3(c_i \cdot u_A)}{c^2} + \frac{9(c_i \cdot u_A)^2}{2c^4} - \frac{3u_A^2}{2c^2}\right] \quad (3)$$

$$g_{Bi}^{eq} = \omega_i C_B\left[1 + \frac{3(c_i \cdot u_A)}{c^2}\right] \quad (4)$$

where lattice velocity $c = \Delta x/\Delta t$ is set to unity; and ω_i ($i = 1$–9) are the weight factors for D2Q9: $\omega_9 = 4/9$, $\omega_1 = \omega_2 = \omega_3 = \omega_4 = 1/9$, and $\omega_5 = \omega_6 = \omega_7 = \omega_8 = 1/36$.

The discrete velocities, $\mathbf{c}_i$ ($i = 1$–9), for D2Q9 are defined as follows:

$$c_i = \begin{cases} \left(\cos\left(\frac{(i-1)\pi}{2}\right), \sin\left(\frac{(i-1)\pi}{2}\right)\right) & i = 1\text{–}4 \\ \sqrt{2}\left(\cos\left(\frac{(i-5)\pi}{2} + \frac{\pi}{4}\right), \sin\left(\frac{(i-5)\pi}{2} + \frac{\pi}{4}\right)\right) & i = 5\text{–}8 \\ (0, 0) & i = 9 \end{cases} \quad (5)$$

The macroscopic quantities such as solvent density ρ_A, macroscopic velocity $\boldsymbol{u}_A$ and solute concentration C_B are

Table 1 – Physical properties of pure solvents and saturated solutions at 298.15 K, 1.00 atm.

Solvents	ρ_0 (kg m^{-3})	$\Delta\rho$ (kg m^{-3})	C^* (kg m^{-3})	$10^9 D_l$ (m^2 s^{-1})	$10^3\mu_0$ (Pa s)	H (Pa m^3 mol^{-1})
Ethanol	785.22[a]	1.01[e]	4.70[g]	3.86[g]	1.08[g]	9.49×10^2
Methanol	786.48[b]	1.45[e]	6.25[g]	5.13[j]	0.55[g]	7.13×10^2
Water	997.04[a]	0.38[f]	1.50[h]	2.00[h]	0.89[j]	2.97×10^3
Benzene	873.70[c]	0.18[e]	4.09[g]	3.85[g]	0.60[g]	1.09×10^3
Toluene	862.20[d]	0.49[e]	4.45[i]	4.60[k]	0.56[d]	1.00×10^3

[a] From Arce et al. (2000).
[b] From Chen et al. (2002).
[c] Aralaguppi et al. (1999).
[d] From Nikam and Kharat (2005).
[e] From Okhotsimskiis and Hozawa (1998).
[f] From Tan and Thorpe (1999).
[g] From Takahashi and Kobayashi (1982).
[h] From Versteeg and Swaaij van (1988).
[i] From Perisanu (2001).
[j] From Frank et al. (1996).
[k] From McManamey and Woollen (1973). H obtained by C^* and p approximately followed Henry's law.

defined in terms of the particle distribution function as follows:

$$\rho_A = \sum_{i=1}^{9} f_{Ai}, \quad u_A = \frac{1}{\rho_A}\sum_{i=1}^{9} c_i f_{Ai}, \quad C_B = \sum_{i=1}^{9} g_{Bi} \tag{6}$$

The liquid viscosity and diffusivity coefficient of the solute in the liquid are defined by (Inamuro et al., 2002):

$$\nu = \frac{1}{3}c^2\Delta t(\tau_A - 0.5) \tag{7}$$

$$D_l = \frac{1}{3}c^2\Delta t(\tau_B - 0.5) \tag{8}$$

By these definitions and with ν and D for given species, parameters τ_A and τ_B can be evaluated.

2.3. Implementation of external forces

The assumption of Boussinesq approximation (Shan, 1997) is adopted so that the fluid properties, except the density, such as the viscosity and diffusivity coefficient are assumed to be independent of concentration. Thus, only the body force, gravity or buoyancy, caused by density difference is considered as external force in the system. Then, the density difference that we assumed to vary linearly with the concentration difference caused by the mass transfer is the only source of the external forces. Similar to processing method for body force in the Rayleigh–Bénard convection induced by temperature gradient (Shan, 1997), the body force per unit volume of Rayleigh convection is approximately given by:

$$\mathbf{F} = -\frac{\Delta\rho}{\Delta C}(C_B - C_0)g \tag{9}$$

Incorporating the body force into the model, the velocity in the equilibrium distribution function $\mathbf{u}^*$ and flow velocity $\mathbf{u}$ are modified as follows (Buick and Greated, 2000):

$$\mathbf{u}^* = \mathbf{u}_A + \tau_A\frac{\mathbf{F}\Delta t}{\rho_A} \tag{10}$$

$$\mathbf{u} = \mathbf{u}_A + \frac{1}{2}\frac{\mathbf{F}\Delta t}{\rho_A} \tag{11}$$

2.4. Boundary conditions

The bounce-back boundary and periodic boundary are employed respectively on the lower boundary and on the left and right walls of the computational domain, for both the flow and concentration fields.

A constant concentration boundary (Sukop and Thorne, 2006) is used on the gas–liquid interface. As theoretically reasoned and suggested by Kim et al. (2006), the buoyancy-driven convection phenomena in gas absorption should be modeled as a constant liquid surface concentration system. This corresponds physically well to the transport process under consideration in the present work. For the mass transfer process where the gas phase is pure (or nearly pure) carbon dioxide, the mass transfer is known to be controlled by the liquid side resistance. In such a case the liquid surface (the interface) can be safely assumed to be in phase equilibrium with the gas, the concentration of which is independent of the interfacial mass transfer. Tan and Thorpe (1999) have also given a simple criterion to determine whether a constant concentration or a constant flux models should be used at the boundary of the liquid surface. According to the criterion that was defined by a transient Biot number $Bi_D = H(D_g/D_l)^{1/2}/(RT)$, where D_g is the self-diffusion coefficient of CO_2 and is equal to 1.25×10^{-5} m^2 s^{-1} at 298.15 K (Tan and Thorpe, 1999) and D_l is the diffusion coefficient of CO_2 in the liquid, a good approximation of fixed surface concentration boundary and constant mass flux boundary could be guaranteed if Bi_D is greater than 10 and less than 1, respectively. According to the Biot number given in Table 2, the constant concentration boundary can be adopted on the gas–liquid interface for CO_2 absorption into the solvents listed in the table. It should be noted that Tan and Thorpe's criterion (Tan and Thorpe, 1999) could not always give a consistent result with that given by Kim et al. (2006).

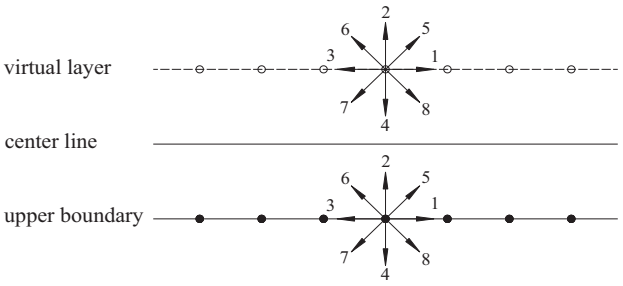

Fig. 3 – Schematic diagram of mirror symmetric boundary based on D2Q9 model.

At the upper boundary for the flow field, a mirror symmetric boundary (Shi et al., 2006) is used to treat the gas–liquid free interface. Such a boundary condition can ensure a zero horizontal velocity gradient in vertical direction. This can be achieved by adding a virtual layer of nodes above that of the upper boundary as shown in Fig. 3, and the distribution functions at the nodes on the virtual layer are symmetrically equal to the distribution functions on the upper boundary.

2.5. Modeling of interfacial disturbance

In addition to Rayleigh instability, interfacial disturbance is a necessary condition of occurrence of Rayleigh convection. In the real gas–liquid mass transfer process, the mechanism of the interfacial disturbance is complex and randomly featured. For the isothermal mass transfer process in a quiescent gas–liquid system in the present study the disturbances may regard solely concentration perturbation. In order to model the process of concentration perturbations, we propose to use two parameters to capture the random features: P the possibility of occurrence of concentration perturbation at any given position on the liquid surface and C_D the concentration perturbation magnitude. To implement the two-parameter perturbation model in our LBM after each time step Δt, C_l' the

Table 2 – Transient Biot numbers for CO_2 diffusion in various solvents at 298.15 K.

Parameter	Ethanol	Methanol	Water	Benzene	Toluene
Bi_D	21.78	14.20	94.72	25.06	21.03

concentration at any lattice node at the liquid surface is given by Eq. (12); and a random number is generated for that node. If the random number is smaller than P, then concentration perturbation $\delta C = \pm C_D$, otherwise $\delta C = 0$.

$$C_I' = C_I + \delta C \tag{12}$$

Thus, the model gives such a picture: at any position and time on the gas–liquid interface, the liquid concentration perturbation occurs with probability P and magnitude C_D.

3. Identification of parameters P and C_D

In this section, the values of parameters P and C_D are identified by comparing our simulated results with the experiments by Blair and Quinn (1969) and the theoretical predictions by Kim et al. (2006) and Tan and Thorpe (1999) on the critical onset time of Rayleigh convection. The gas–liquid mass transfer processes of CO_2 absorption into water and ethanol are used for the simulation and comparison.

In the simulation, the interfacial concentration is set as the equilibrium concentration for CO_2 in various solvents at 298.15 K, 1.00 atm. The dimensions of the simulation domains are chosen as 5 mm × 5 mm (h = 5 mm), which can accommodate the observable development of Rayleigh convection. The grid size is set to 3.33 mm × 10^{-2} mm, balancing the accuracy of computing results and the computational cost.

3.1. *Simulation of Rayleigh convection*

3.1.1. *Unperturbed interface*

Fig. 4 shows the transient contour line of CO_2 concentration without perturbation (P = 0 and/or C_D = 0) at t = 300 s in the process of CO_2 absorption into ethanol. As can be seen, the interfacial mass transfer only proceeded in the manner of molecular diffusion; and the Rayleigh convection would not occur even in presence of Rayleigh instability generated by the concentration gradient shown in Fig. 4.

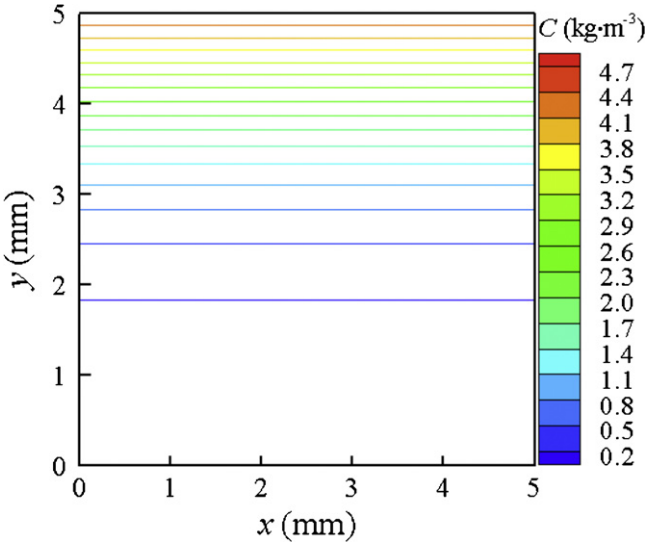

Fig. 4 – Transient contour line of CO_2 concentration without disturbance at t = 300 s in the process of CO_2 absorption into ethanol.

3.1.2. *Critical onset time of Rayleigh convection*

In this study, the critical onset time of Rayleigh convection was obtained by observing the development of the concentration contour line and the deviation of instantaneous mass flux across the interface from the theoretical value predicted by penetration theory.

Fig. 5 shows the transient contour lines of CO_2 concentration after 35 s, 45 s, 52 s and 60 s with P = 0.06, $C_D = 10^{-12}$ kg m^{-3} in the process of CO_2 absorption into ethanol. The CO_2 concentration gradient in the vicinity of the interface yielded the unstable adverse density gradient as shown in Fig. 5(A). Then, the deformation of the contour lines appeared and developed into convection (Fig. 5(B)–(D)), and the critical onset time of Rayleigh convection was found to be approximately 52 s.

From the concentration field by the simulation, the instantaneous mass flux $N_{ins,t}$ across the interface at time t can be estimated:

$$N_{ins,t} = \frac{(C_{avg,t+\delta t} - C_{avg,t})V}{(A_I \delta t)} = \frac{(C_{avg,t+\delta t} - C_{avg,t})h}{\delta t} \tag{13}$$

where the time interval δt was set to 0.1 s, which is far less than the simulated critical onset time of Rayleigh convection.

The instantaneous mass flux across the interface $N^0_{inst,t}$ according to penetration theory is given by (Cussler, 2009):

$$N^0_{ins,t} = \sqrt{\frac{D}{\pi t}}(C_I - C_0) \tag{14}$$

The variation of instantaneous mass flux across the interface with time t with P = 0.06, $C_D = 10^{-12}$ kg m^{-3} in the process of CO_2 absorption into ethanol is shown in Fig. 6. As shown in Fig. 6, the instantaneous mass flux aross the interface is continually decreased before 52 s wherein the interfacial mass transfer only proceeds in the way of molecular diffusion. It can be found that the simulation results agree very well with the values perdicted by the penetration theory within that time period. Around 52 s, the instantaneous mass flux across the interface increases sharply, indicating the onset of Rayleigh convection. Following that, the interfacial mass transfer can be known as being dominated by the Rayleigh convection. As a result, the instantaneous mass flux across the interface after 52 s is well above that derived from penetration theory and thereby the critical onset time of Rayleigh convection can be identified.

3.2. *Theoretical prediction of onset of Rayleigh convection*

A theoretical prediction of critical time of onset of Rayleigh convection deduced by Kim et al. (2006) based on a linear stability theory (propagation theory) is given by:

$$t_{c0} = 7.38\left(\frac{\mu}{gC_I\sqrt{D}\Delta\rho/\Delta C}\right)^{2/3} \tag{15}$$

Kim et al. (2006) pointed out that, although Eq. (15) was deduced for a rigid liquid surface boundary condition, some in-depth comparison with experiments (Blair and Quinn, 1969; Mahler and Schechter, 1970) indicated its applicability to free water surface cases. Note that, according to propagation theory, the critical onset time t_{c0} given by Eq. (15) is theoretically defined as the time at which infinitesimal concentration disturbances are propagated, within a length scaling all the

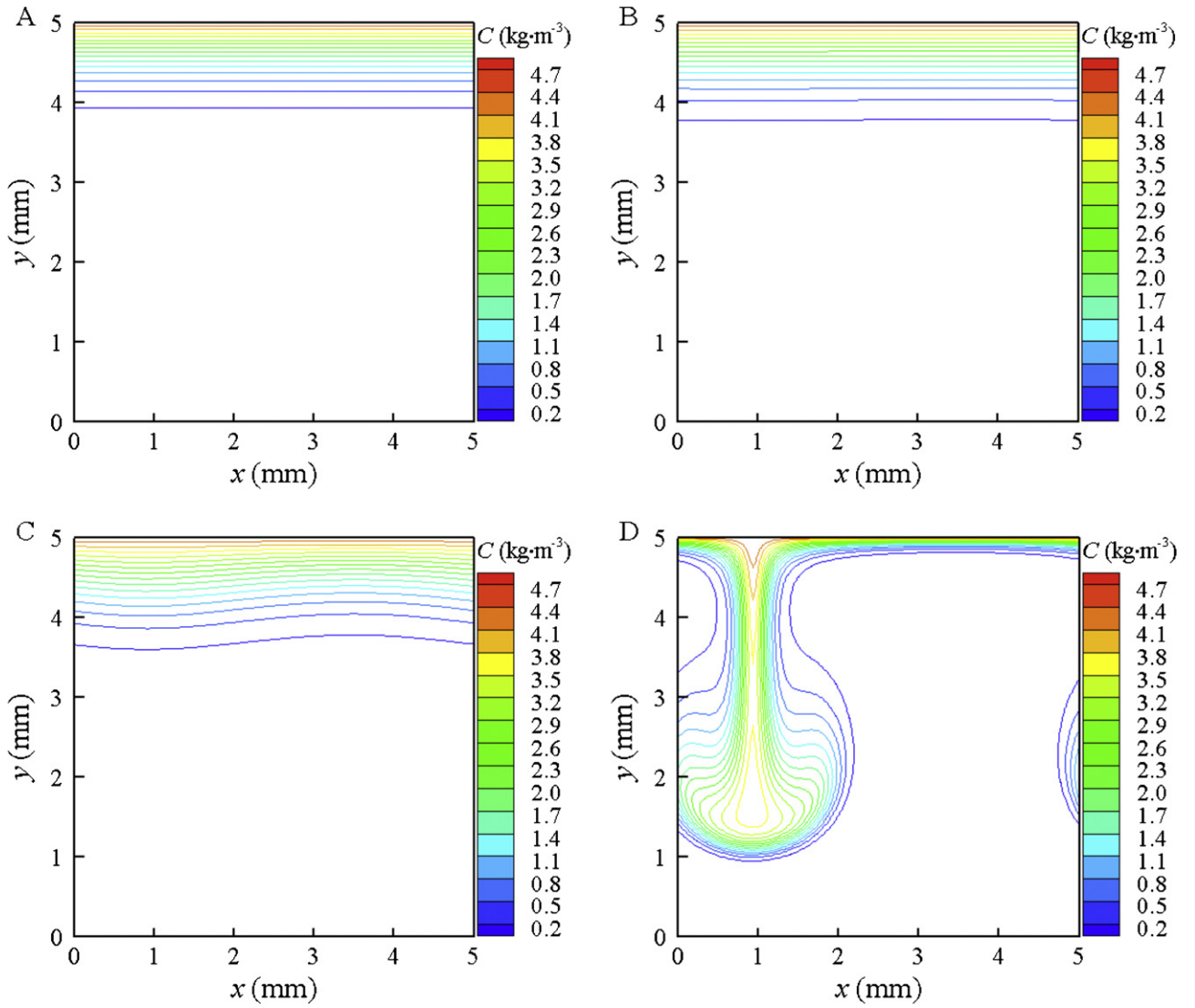

Fig. 5 – Transient contour lines of CO_2 concentration after 35 s (A), 45 s (B), 52 s (C) and 60 s (D) with $P = 0.06$, $C_D = 10^{-12}$ kg m^{-3} in the process of CO_2 absorption into ethanol.

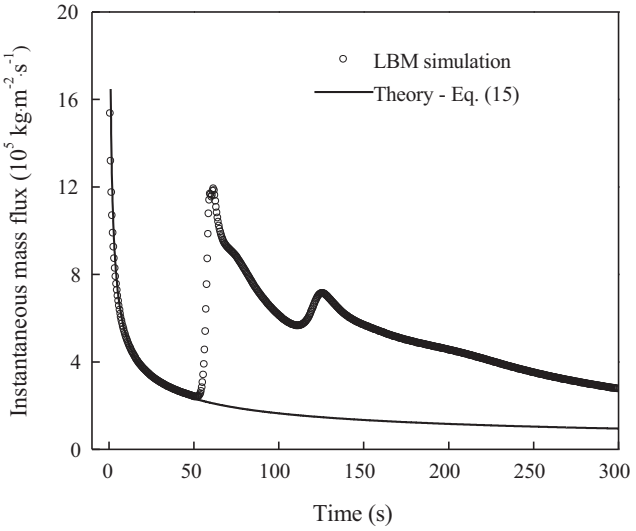

Fig. 6 – Variation of instantaneous mass flux across the interface with time with $P = 0.06$, $C_D = 10^{-12}$ kg m^{-3} in the process of CO_2 absorption into ethanol.

variables and parameters (Kim et al., 2006). As mentioned by Foster (1969) and suggested by Kim et al. (2006), a critical time to make the onset of detectable (manifest) Rayleigh convection t_c should be four times longer as t_{c0}, that is

$$t_c = 4t_{c0}. \tag{16}$$

Tan and Thorpe (1992, 1999) have also developed a maximum Rayleigh number criterion for the onset of Rayleigh convection in the liquid layer evoked by unstable transient mass transfer. Assuming that the concentration gradient in the liquid can be represented by the penetration theory, they defined a transient Rayleigh number as a function of z as follows:

$$Ra_z = \left(\frac{\Delta\rho}{\Delta C}\right)\frac{gz^4 C_I}{\mu\sqrt{\pi D^3 t}}\exp\left(\frac{-z^2}{4Dt}\right) \tag{17}$$

The maximum transient Rayleigh number at any specified time t can be derived by differentiating Eq. (17) and setting the differentiation equal to zero, which yields a maximum

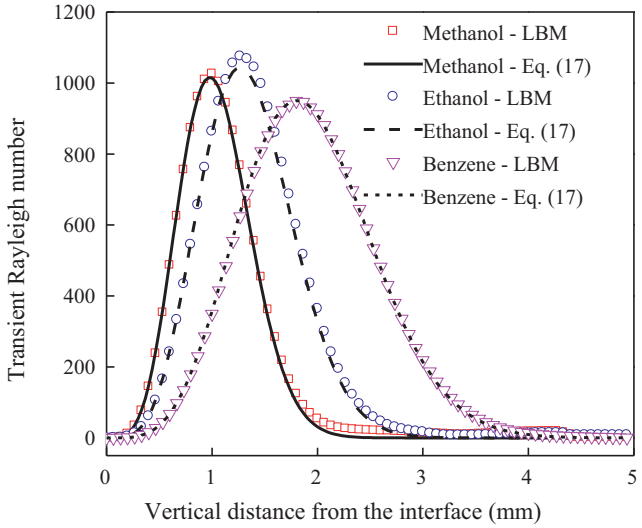

Fig. 7 – Comparison of predicted and simulated variations of transient Rayleigh number with vertical distance from the interface for CO_2 absorption into various solvents at critical onset times ($P = 0.06$, $C_D = 10^{-12}$ kg m^{-3} for simulation).

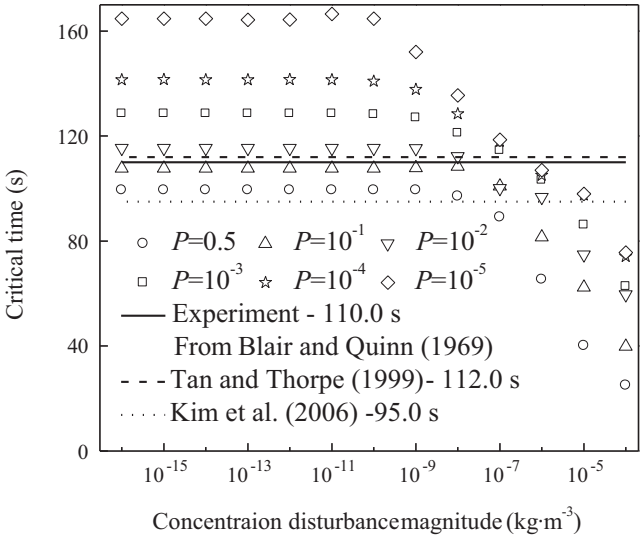

Fig. 8 – Variation of critical onset times of Rayleigh convection with concentration perturbation magnitude for different P in the process of CO_2 absorption into water.

penetration depth $z_{max} = 2\sqrt{2Dt}$. Then, the maximum transient Rayleigh number can be found at z_{max}:

$$Ra_{max} = \frac{4.89 g C_I \sqrt{Dt^3}}{\mu}\left(\frac{\Delta\rho}{\Delta C}\right) \quad (18)$$

According to Tan and Thorpe (1992, 1999), Rayleigh convection occurs when the maximum transient Rayleigh number reaches a critical Rayleigh number Ra_c, which was given by Sparrow et al. (1964). Thus, the critical onset time can be given as:

$$t_c = \left(\frac{\mu Ra_c/4.89}{g C_I \sqrt{D}\Delta\rho/\Delta C}\right)^{2/3} \quad (19)$$

The variations of transient Rayleigh number Ra_z with vertical distance from the interface z given by Eq. (17) for CO_2 absorption into various solvents at critical onset times t_c determined by Eq. (15) with the value of Ra_c given in Sparrow et al. (1964) are shown in Fig. 7. The transient Rayleigh numbers increase first and then decrease after reaching the maximum value of Ra_{max} given by Eq. (18).

3.3. *Parameter identification for random perturbation model*

Our identification of the parameters, the probability and magnitude of the concentration perturbation, starts with CO_2–water absorption, the critical Rayleigh number of which is given in Table 2. Fig. 8 shows the variation of critical onset times of Rayleigh convection with the magnitude C_D for different probability P in the process of CO_2 absorption into water by our LBM simulation. As can be seen in Fig. 8, the critical onset time for any given P, was shown to be independent of concentration perturbation magnitude if $0 < C_D \le 10^{-9}$ kg m^{-3}. Then, the variation of t_c with P for the particular $C_D = 10^{-12}$ kg m^{-3} (this is well within the stable domain of $0 < C_D \le 10^{-9}$ kg m^{-3}) is given in Fig. 9. The experimental critical onset time from Blair and Quinn (1969), the theoretical predictions of t_c by Eqs. (16) and (19) with a critical Rayleigh number $Ra_c = 1084$ (Sparrow et al., 1964) are also marked in Figs. 8 and 9. It can be seen firstly from the figures that the theoretical results given by Kim et al. (2006) and Tan and Thorpe (1999) agree well with the experimental results for CO_2–water absorption, but with the prediction by Eq. (19) fairly closer to the experimental results. Secondly, the value of parameter P should be suitably identified as $0.05 \le P \le 0.3$ according to the figures.

For the process of CO_2 absorption into ethanol, the simulation results on the dependence of the critical onset time of Rayleigh convection on the parameters of P and C_D are shown in Figs. 10 and 11, respectively. At the same time, the predicted t_c by Eqs. (16) and (19) with the critical Rayleigh number $Ra_c = 1028$ (Sparrow et al., 1964) are also marked in Figs. 10 and 11. It can be seen that the dependences of t_c on the parameters P and C_D for the CO_2–ethanol absorption showed the same patterns as those for the case of CO_2–water absorption. First, like that for CO_2–water system, the value of C_D should be identified as $0 < C_D \le 10^{-9}$, say $C_D = 10^{-12}$ kg m^{-3} as suggested by Fig. 10. In identifying parameter P, however,

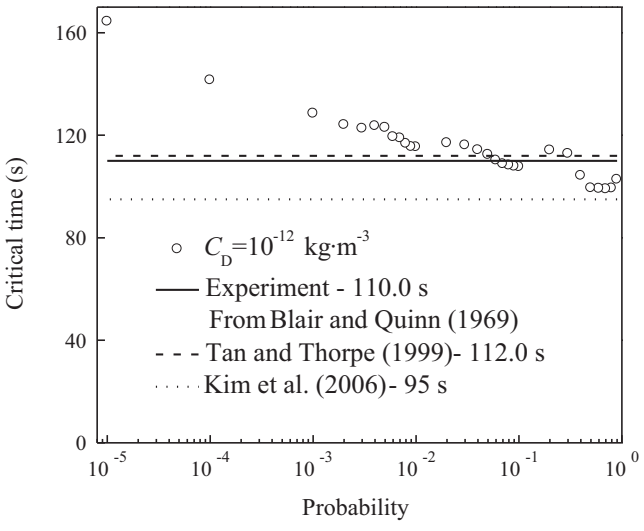

Fig. 9 – Variation of critical onset times of Rayleigh convection with perturbation probability at $C_D = 10^{-12}$ kg m^{-3} in the process of CO_2 absorption into water.

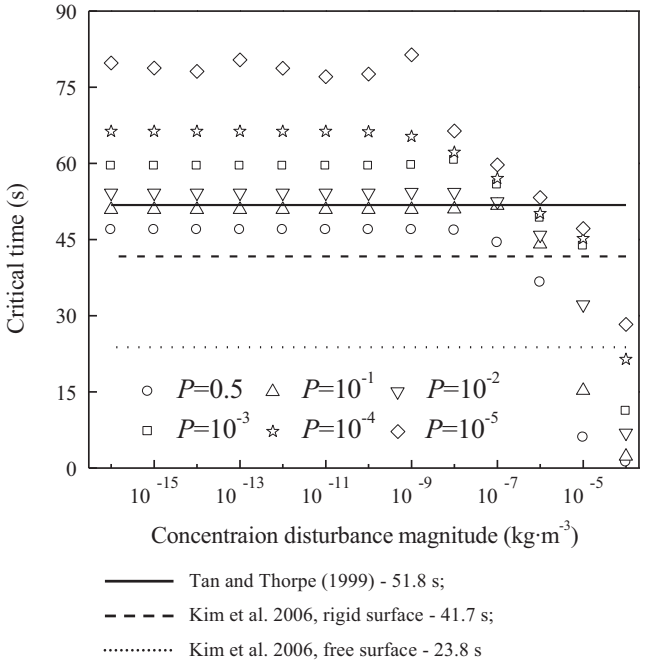

Fig. 10 – Variation of critical onset times of Rayleigh convection with concentration perturbation magnitude for different P in the process of CO_2 absorption into ethanol.

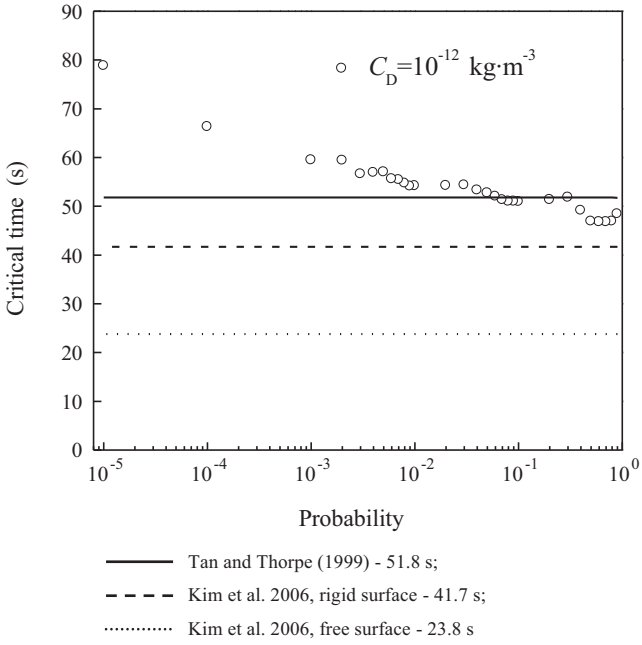

Fig. 11 – Variation of critical onset times of Rayleigh convection with perturbation probability at $C_D = 10^{-12}$ kg m^{-3} in the process of CO_2 absorption into ethanol.

the corresponding critical times calculated by Eqs. (16), (19) and (15) show a large deviation. It should be pointed out that Eq. (16) was developed for a rigid surface boundary condition, and for a free surface condition, the critical onset time should be 23.8 s [see Eq. (37) in Kim et al. (2006)], even much smaller than that predicted by Eqs. (19) and (16) as well (see Figs. 10 and 11). By comparing Figs. 8 and 9 with Figs. 10 and 11, the prediction by Eq. (19) is shown to be more consistent, and then was suitably used to identify parameter P in our work. As shown in Figs. 8–11, according to such predicted critical time, it can be seen that identical values of P and C_D ($0.05 \le P < 0.3$ and $0 < C_D \le 10^{-9}$ kg m^{-3}) can be obtained for both CO_2–water and CO_2–ethanol systems.

Table 3 shows the comparisons of the simulated and predicted maximum penetration depth, maximum transient Rayleigh number, and critical onset time of Rayleigh convection for CO_2 diffusion in various solvents at 298.15 K, 1.00 atm with the identified values of the parameter $P = 0.06$, $C_D = 10^{-12}$ kg m^{-3} which are well within the identified scope ($0.05 \le P < 0.3$ and $0 < C_D \le 10^{-9}$ kg m^{-3}). The maximum penetration depths and the critical onset times of Rayleigh convection are found to be well consistent with the predicted values from the theory of Tan and Thorpe (1992, 1999), and the maximum transient Rayleigh numbers are also found to be in good agreement with the theoretical critical Rayleigh numbers obtained by Sparrow et al. (1964), where the maximum errors are not beyond 3.17%, 4.46% and 4.34%, respectively.

Variations of transient Rayleigh number with vertical distance from the interface at critical onset times given by LBM simulation with $P = 0.06$, $C_D = 10^{-12}$ kg m^{-3} are shown in Fig. 7. And the simulated transient Rayleigh numbers can be found to be in good agreement with the predicted values by the theory of Tan and Thorpe (1992, 1999), which further justifys our simulated results.

4. The effect of Rayleigh convection on interfacial mass transfer

In this section we apply the random perturbation model developed in the previous sections in an expanded computational domain of 20 mm × 5 mm ($h = 5$ mm) to investigate the development of multiple plume convection patterns. As simulated results, Figs. 12–14 describe the transient contours of CO_2 concentration, velocity fields and streamlines respectively at different time in the gas–liquid mass transfer process of CO_2 absorption into ethanol with the identified parameters $P = 0.06$, $C_D = 10^{-12}$ kg m^{-3}.

Table 3 – Comparisons of the simulated and predicted maximum penetration depth z_{max}, maximum transient Rayleigh number Ra_{max}, and critical time t_c of the onset of Rayleigh convection for CO_2 diffusion in various solvents at 298.15 K, 1.00 atm.

Solvents	Simulated z_{max} (mm)	Predicted z_{max} (mm)	Simulated Ra_{max}	Predicted Ra_c (= Ra_{max})[a]	Simulated t_c (s)	Predicted t_c (s)
Ethanol	1.30	1.26	1076	1028	52.0	51.8
Methanol	1.00	0.97	1026	1003	23.4	23.1
Water	1.37	1.34	1065	1084	110.2	112.0
Benzene	1.83	1.85	1021	1039	105.9	110.7
Toluene	1.37	1.37	996	1026	50.2	50.7

[a] Ra_c data obtained from Sparrow et al. (1964)

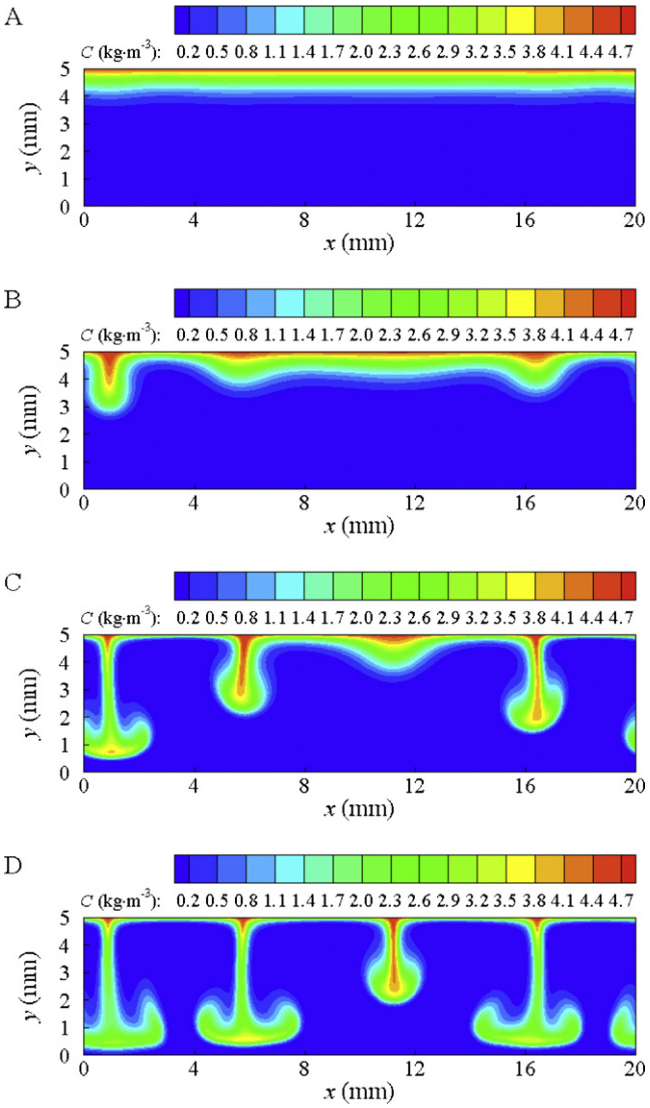

Fig. 12 – Transient contours of CO_2 concentration after 52 s, 58 s, 62 s and 66 s in the process of CO_2 absorption into ethanol.

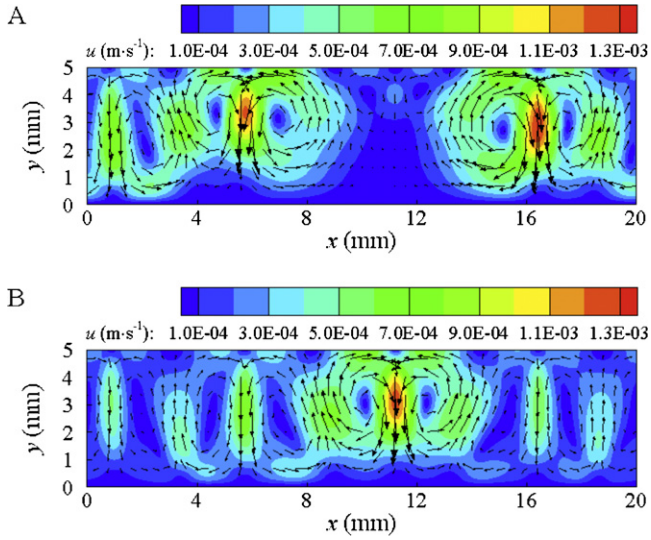

Fig. 13 – Transient velocity fields after 62 s and 66 s in the process of CO_2 absorption into ethanol.

As can be seen in Fig. 12, the Rayleigh convection begins near the interface at 52 s. Then the Rayleigh convection gives rise to violent intermittent eruptions from randomly localized positions at the interface. After that, the liquid with higher concentration begins to stream downward in a plume convection pattern combined with molecular diffusion, and then the plumes swing back and forth when they reach the bottom. The concentration contours simulated are well consistent with typical plume convection patterns reported in literatures (Okhotsimskiis and Hozawa, 1998; Kutepov et al., 2001).

As shown in Figs. 13 and 14, there are several pairs of roll cells with diverse rotational directions and different sizes in the liquid bulk. The velocities in the regions of Rayleigh convection are relatively high (10^{-4}–10^{-3} m s^{-1}) and the order of magnitude is the same as the experimental data reported by Chen (2010) and Fu et al. (2011). The circulation flows with high velocity and vortexes impel the exchange of the liquid between the interfacial vicinity and the liquid bulk and thus promote the renewal of interfacial liquid.

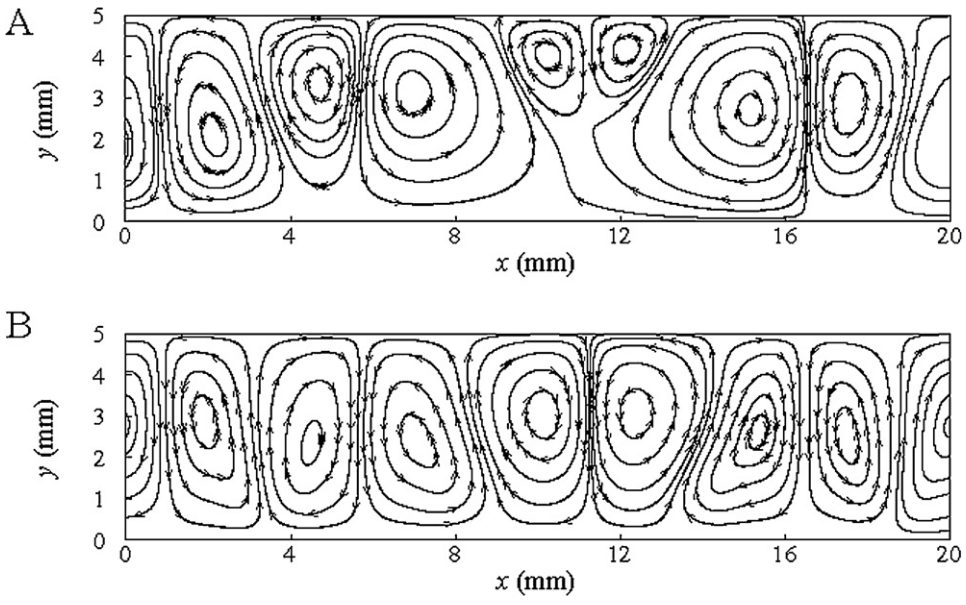

Fig. 14 – Transient streamlines after 62 s and 66 s in the process of CO_2 absorption into ethanol.

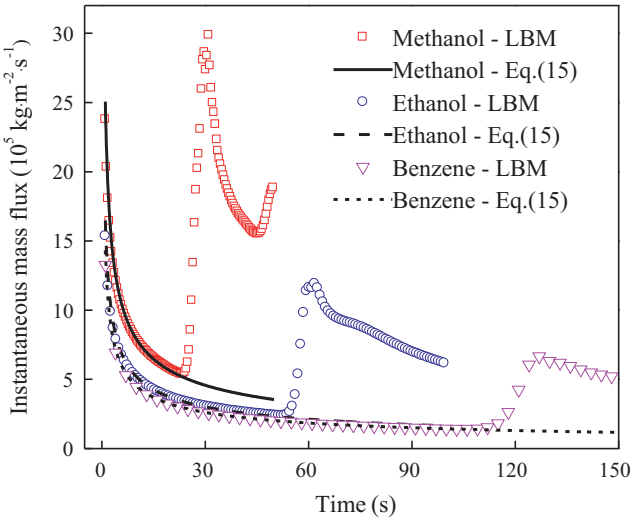

Fig. 15 – Variation of instantaneous mass flux across the interface with time for CO_2 absorption into various solvents.

Variations of instantaneous mass flux across the interface with time for CO_2 absorption into various solvents are shown in Fig. 15. The difference in critical onset times of Rayleigh convection for different solvents can be clearly seen in Fig. 15. Comparing the simulated instantaneous mass flux across the interface and that of penetration theory, it can be seen that the liquid-phase mass transfer rate is effectively enhanced.

5. Conclusions

The established LBM with a double distribution model has been used to analyze the two-dimensional liquid-phase Rayleigh convection induced by interfacial mass transfer in gas absorption systems. The key point for this scheme lies in proposing a random perturbation model for evoking the convection. Two parameters, P and C_D, characterizing the possibility and the magnitude of concentration perturbation at any point on the liquid surface were introduced, and the intervals of $0.05 \leq P < 0.3$ and $0 < C_D \leq 10^{-9}$ kg m^{-3} have been identified as the suitable values for the parameters, by comparison of the simulated critical onset times of Rayleigh convection with the experimental value from Blair and Quinn (1969) and the theoretical values obtained by Kim et al. (2006) and Tan and Thorpe (1992, 1999).

The simulated results with the proposed model show that the Rayleigh convection will not occur if the gas–liquid interface is unperturbed, and in case of the disturbance the Rayleigh convection appears when the depth of solute penetration from the interface exceeds a critical value. Concentration contours in the presence of Rayleigh convection obtained by our simulation are well consistent with plume convection patterns reported in literatures. The simulation method proposed can be used to give instantaneous mass flux across the interface, and it can be seen from the results that the liquid-phase mass transfer rate is effectively enhanced by Rayleigh convection. It can be seen clearly that the enhancement of mass transfer can be attributed to circulation flows with high velocity and vortexes in the liquid bulk, which impel the exchange of the liquid between the interfacial vicinity and the liquid bulk and promote the renewal of interfacial liquid.

Acknowledgement

The authors wish to acknowledge the financial support from the National Natural Science Foundation of China (No. 20736005).

References

Aralaguppi, M.I., Jadar, C.V., Aminabhavi, T.M., 1999. Density, refractive index, viscosity, and speed of sound in binary mixtures of cyclohexanone with benzene, methylbenzene, 1,4-dimethylbenzene, 1,3,5-trimethylbenzene, and methoxybenzene in the temperature interval (298.15–308.15) K. J. Chem. Eng. Data 44, 446–450.

Arce, A., Arce Jr., A., Rodil, E., Soto, A., 2000. Density, refractive index, and speed of sound for 2-ethoxy-2-methylbutane + ethanol + water at 298.15 K. J. Chem. Eng. Data 45, 536–539.

Arendt, B., Dittmar, D., Eggers, R., 2004. Interaction of interfacial convection and mass transfer effects in the system CO_2–water. Int. J. Heat Mass Transfer 47, 3649–3657.

Bhatnagar, P.L., Gross, E.P., Krook, M., 1954. A model for collision processes in gases. I. Small amplitude processes in charged and neutral one-component systems. Phys. Rev. 94, 511–525.

Barbosa, J.R., Thoma, S.M., Marcelino Neto, M.A., 2008. Prediction of refrigerant absorption and onset of natural convection in lubricant oil. Int. J. Refrig. 31, 1231–1240.

Buick, J.M., Greated, C.A., 2000. Gravity in a lattice Boltzmann model. Phys. Rev. E 61, 5307–5320.

Blair, L.M., Quinn, J.A., 1969. The onset of cellular convection in a fluid layer with time-dependent density gradients. J. Fluid Mech. 36, 385–400.

Chang, Q., Alexander, J.I.D., 2006. Application of the lattice Boltzmann method to two-phase Rayleigh–Bénard convection with a deformable interface. J. Comput. Phys. 212, 473–489.

Chen, S., Lei, Q., Fang, W., 2002. Density and refractive index at 298.15 K and vapor–liquid equilibria at 101.3 kPa for four binary systems of methanol, n-propanol, n-butanol, or isobutanol with N-methylpiperazine. J. Chem. Eng. Data 47, 811–815.

Chen, W., 2010. Experimental measurement of gas–liquid interfacial Rayleigh–Bénard–Marangoni convection and mass transfer. Ph.D. Thesis, Tianjin University, Tianjin, China.

Cussler, E.L., 2009. Diffusion: Mass Transfer in Fluid Systems, third ed. Cambridge University Press, New York.

Farajzadeh, R., Salimi, H., Zitha, P.L.J., Bruining, H., 2007. Numerical simulation of density-driven natural convection in porous media with application for CO_2 injection projects. Int. J. Heat Mass Transfer 50, 5054–5064.

Farajzadeh, R., Zitha, P.L.J., Bruining, J., 2009. Enhanced mass transfer of CO_2 into water: experiment and modeling. Ind. Eng. Chem. Res. 48, 6423–6431.

Foster, T.D., 1969. Onset of manifest convection in a layer of fluid with a time-dependent surface temperature. Phys. Fluids 12, 2482.

Frank, M.J.W., Kuipers, J.A.M., van Swaaij, W.P.M., 1996. Diffusion coefficients and viscosities of $CO_2 + H_2O$, $CO_2 + CH_3OH$, $NH_3 + H_2O$, and $NH_3 + CH_3OH$ liquid mixtures. J. Chem. Eng. Data 41, 297–302.

Fu, B., Yuan, X.G., Liu, B.T., Chen, S.Y., Zhang, H.S., Zeng, A.W., Yu, G.C., 2011. Characterization of Rayleigh convection in interfacial mass transfer by lattice Boltzmann simulation and experimental verification. Chin. J. Chem. Eng. 19, 845–854.

Grahn, A., 2006. Two-dimensional numerical simulations of Marangoni–Bénard instabilities during liquid–liquid mass transfer in a vertical gap. Chem. Eng. Sci. 61, 3586–3592.

Hassanzadeh, H., Pooladi-Darvish, M., Keith, D.W., 2009. The effect of natural flow of aquifers and associated dispersion on the onset of buoyancy-driven convection in a saturated porous medium. AIChE J. 55, 475–485.

Hidalgo, J.J., Carrera, J., 2009. Effect of dispersion on the onset of convection during CO_2 sequestration. J. Fluid Mech. 640, 441–452.
Inamuro, T., Yoshino, M., Inoue, H., Mizuno, R., Ogino, F., 2002. A lattice Boltzmann method for a binary miscible fluid mixture and its application to a heat-transfer problem. J. Comput. Phys. 179, 201–215.
Kim, M.C., Lee, S.G., 2009. Onset of solutal convection in liquid phase epitaxy system. Korean J. Chem. Eng. 26, 21–25.
Kim, M.C., Yoon, D.Y., Choi, C.K., 2006. Onset of buoyancy-driven instability in gas diffusion systems. Ind. Eng. Chem. Res. 45, 7321–7328.
Kurenkova, N., Eckert, K., Zienicke, E., Thess, A., 2003. Desorption-driven convection in aqueous alcohol solution. Lect. Notes Phys. 628, 403–416.
Kutepov, A.M., Pokusaev, B.G., Kazenin, D.A., Karlov, S.P., Vyaz'min, A.V., 2001. Interfacial mass transfer in the liquid–gas system: an optical study. Theor. Found. Chem. Eng. 35, 213–216.
Ma, C.F., 2009. Lattice BGK simulations of double diffusive natural convection in a rectangular enclosure in the presences of magnetic field and heat source. Nonlinear Anal. Real World Appl. 10, 2666–2678.
Mahler, E.G., Schechter, R.S., 1970. The stability of fluid layer with gas absorption. Chem. Eng. Sci. 25, 955.
McManamey, W.J., Woollen, J.M., 1973. The diffusivity of carbon dioxide in some organic liquids at 25 °C and 50 °C. AIChE J. 19, 667–669.
Mohamad, A.A., El-Ganaoui, M., Bennacer, R., 2009. Lattice Boltzmann simulation of natural convection in an open ended cavity. Int. J. Therm. Sci. 48, 1870–1875.
Mussa, M.A., Abdullah, S., Nor Azwadi, C.S., Muhamad, N., 2011. Simulation of natural convection heat transfer in an enclosure by the lattice-Boltzmann method. Comput. Fluids 44, 162–168.
Okhotsimskiis, A., Hozawa, M., 1998. Schlieren visualization of natural convection in binary gas–liquid systems. Chem. Eng. Sci. 53, 2547–2573.
Nikam, P.S., Kharat, S.J., 2005. Density and viscosity studies of binary mixtures of N,N-dimethylformamide with toluene and methyl benzoate at (298.15, 303.15, 308.15, and 313.15) K. J. Chem. Eng. Data 50, 455–459.
Perisanu, S.T., 2001. Estimation of solubility of carbon dioxide in polar solvents. J. Solution Chem. 30, 183–192.
Poodt, P.W.G., Christianen, P.C.M., van Enckevort, W.J.P., Maan, J.C., Vlieg, E., 2008. The critical Rayleigh number in low gravity crystal growth from solution. Cryst. Growth Des. 8, 2194–2199.
Qian, Y.H., D'Humieres, D., Lallemand, P., 1992. Lattice BGK models for Navier–Stokes equation. Europhys. Lett. 17, 479–484.
Rayleigh, L., 1916. On convection currents in a horizontal layer of fluid when the higher temperature is on the under side. Philos. Mag. 32, 529–546.
Riaz, A., Hesse, M., Tchelepi, H.A., Orr Jr., F.M., 2006. Onset of convection in a gravitationally unstable diffusive boundary layer in porous media. J. Fluid Mech. 548, 87–111.
Shan, X.W., 1997. Simulation of Rayleigh–Bénard convection using a lattice Boltzmann method. Phys. Rev. E 55, 2780–2788.
Sha, Y., Cheng, H., Yu, Y.H., 2002. The numerical analysis of the gas–liquid absorption process accompanied by Rayleigh convection. Chin. J. Chem. Eng. 10, 539–544.
Shi, Y., Zhao, T.S., Guo, Z.L., 2006. Finite difference-based lattice Boltzmann simulation of natural convection heat transfer in a horizontal concentric annulus. Comput. Fluids 35, 1–15.
Sparrow, E.M., Goldstein, R.J., Jonsson, V.K., 1964. Thermal stability in a horizontal fluid layer: effect of boundary conditions and non-linear temperature profile. J. Fluid Mech. 18, 513–528.
Sukop, M.C., Thorne Jr., D.T., 2006. Lattice Boltzmann Modeling: An Introduction for Geoscientists and Engineers. Springer, Berlin.
Sun, Z.F., 2012. Onset of Rayleigh–Bénard–Marangoni convection with time-dependent nonlinear concentration profiles. Chem. Eng. Sci. 68, 579–594.
Sun, Z.F., Fahmy, M., 2006. Onset of Rayleigh–Bénard–Marangoni convection in gas–liquid mass transfer with two-phase flow: theory. Ind. Eng. Chem. Res. 45, 3293–3302.
Sun, Z.F., Yu, K.T., 2006. Rayleigh–Bénard–Marangoni cellular convection expressions for heat and mass transfer rates. Chem. Eng. Res. Des. 84, 185–191.
Sun, Z.F., Yu, K.T., Wang, S.Y., Miao, Y.Z., 2002. Absorption and desorption of carbon dioxide into and from organic solvents: effect of Rayleigh and Marangoni instability. Ind. Eng. Chem. Res. 41, 1905–1913.
Takahashi, M., Kobayashi, Y., 1982. Diffusion coefficients and solubilities of carbon dioxide in binary mixed solvents. J. Chem. Eng. Data 27, 328–331.
Tan, K.K., Tan, Y.W., Choong, T.S.Y., 2009. Onset of natural convection induced by bottom-up transient mass diffusion in porous media. Powder Technol. 191, 55–60.
Tan, K.K., Tey, B.T., Tan, Y.W., 2010. Onset of natural convection in gas–gas system induced by bottom-up transient mass diffusion. Eng. Appl. Comput. Fluid Mech. 4, 475–482.
Tan, K.K., Thorpe, R.B., 1992. Gas diffusion into viscous and non-Newtonian liquids. Chem. Eng. Sci. 47, 3565–3572.
Tan, K.K., Thorpe, R.B., 1999. The onset of convection induced by buoyancy during gas diffusion in deep fluids. Chem. Eng. Sci. 54, 4179–4187.
Verhaeghe, F., Blanpain, B., Wollants, P., 2007. Lattice Boltzmann method for double-diffusive natural convection. Phys. Rev. E 75, 046705.
Versteeg, G.F., van Swaaij, W.P.M., 1988. Solubility and diffusivity of acid gases (CO_2, N_2O) in aqueous alkanolamine solution. J. Chem. Eng. Data 33, 29–34.